Radiation Physics and Chemistry 164 (2019) 108383

Contents lists available at ScienceDirect

Radiation Physics and Chemistry

journal homepage: www.elsevier.com/locate/radphyschem

Radiation effect on the UV-green thermally stimulated luminescence emission of a natural Na-rich aluminosilicate

V. Correcher[a,*], J. Garcia-Guinea[b], C. Boronat[a], J.M. Gómez-Ros[a]

[a] CIEMAT. Av. Complutense 40, 28040, Madrid, Spain
[b] MNCN-CSIC. C/ J. Gutiérrez Abascal 2, 28006, Madrid, Spain

ARTICLE INFO

Keywords:
Retrospective dosimetry
Thermoluminescence
Plagioclase
Structural defects
Activation energy

ABSTRACT

This paper reports on the thermoluminescence (TL) emission (from 250 to 500 nm) of a 10 Gy irradiated natural Na-rich aluminosilicate from Minas Gerais (Brazil), previously characterized by Raman spectroscopy and differential thermal analysis techniques. 3D-TL spectrum of the analyzed sample displays a complex glow curves with five different emissions bands peaked at 290, 380, 420, 460 and 500 nm that could be associated with structural and point defects. The UV-blue emission bands have the following characteristics: (i) the 290 nm waveband could be due to defects-sites by the presence of Na ions; (ii) the 380 nm band, caused by intrinsic defects in the lattice (i.e. Non-Bridging Oxygen Hole Centers (NBOHCs), $[AlO_4]^o$ centres, alkali planar defects and Oxygen Defect Centers (ODCs), among others); (iii) the 420 nm waveband, linked to the recombination on a centre formed from a hole-oxygen atom adjacent to two aluminum atoms (Al-O-Al) and Al-O-Si complexes; (iv) the 460 nm band, associated with the presence of Ti^{4+} in the plagiclase crystal lattice. The green waveband could be linked to de-excitation of Mn^{2+} ions. The estimation of the activation energy (E_a) from the 10 Gy-induced TL glow curves analyzed by means of the initial rise method display linear regressions with acceptable r coefficients ($r > 0.977$) that reveal three groups of components with traps at different depth in the crystal lattice of the albite with Ea values in the range of 0.5–0.64 eV.

1. Introduction

Feldspars in general and plagioclases in particular display well-known cathodo-, radio- (Correcher et al., 2007a), photo- (Cruz-Zaragoza et al., 2015) and thermoluminescence (TL) emission (Correcher et al., 2004). These luminescence properties are mainly due to the intrinsic and extrinsic defects (i.e. point defects, vacancies, Schottky and Frenkel defects, dislocations, planar defects, etc.) inside the crystal lattice, where the emission linked to point defects usually appears at lower energies (over 500 nm) and the structural defects are associated with lower wavebands (in the UV-green region) (Correcher et al., 2011). Studies performed in our laboratory employing different alkali-rich feldspars indicate that are suitable materials as dosimeters due to its acceptable radiation sensitivity, linear dose response (up to 100 Gy), high reproducibility and stability of the signal (Correcher et al., 2004), etc. Such behaviour indicates that can be potentially employed not only in retrospective dosimetry (Bailiff et al., 2004, 2005), radiological terrorism (Jeong et al., 2013), luminescence dating (Aitken, 1985; Krbetschek et al., 1997), detection of irradiated food (Rodriguez-Lazcano et al., 2013), but also for material characterization (Almeida et al., 2018). Specifically, TL of alkali-rich silicates is of interest to obtain information about the trapped charge recombination sites connected with metastable defects inside the lattice that rely on the trapping-detrapping processes during the readout since the structure and the luminescence spectrum are not modified in shape in the temperature range (up to 500 °C) (McKeever, 1986); only some changes in the TL sensitivity could be detected for temperatures lower than 300 °C (Gonzalez and Correcher, 2014). All the factors involved in the TL phenomena (i.e. efficiency, lifetime, emission spectra, etc.) depend directly on the crystalline phase, which is mainly affected by pressure and temperature. Therefore, small alterations in the lattice, such as impurities, surface defects in ppm concentrations, inclusions and substituted ions, among others, could modify not only intensity values, but also wavelength spectral position. Additionally, the shape (Full Width at Half Maximum –FWHM-), intensity (in arbitrary units) and position (maximum of the temperature –T_{max}-) of the TL peaks at a fixed wavelength allow us to get information about the kinetic parameters involving activation energy (E_a), pre-exponential factor (s) and/or kinetic order (b) values that can be calculated using the Glow Curve Fitting (GCF) (Muñiz et al., 1995; Gomez-Ros et al., 2002), Whole Glow Peak

* Corresponding author.
E-mail address: v.correcher@ciemat.es (V. Correcher).

https://doi.org/10.1016/j.radphyschem.2019.108383
Received 6 May 2019; Received in revised form 13 June 2019; Accepted 23 June 2019
Available online 24 June 2019
0969-806X/

(WGP) (Kalita and Chithambo, 2017), Peak Shape (PS) (Aslar et al., 2017; Keskin et al., 2018), Variable Heating Rate (VHR) (Topaksu et al., 2015; Aslar et al., 2017) and Initial Rise (IR) method (Chen and McKeever, 1997; Correcher et al., 2008), among others. The main advantage of the last method is that the E_a parameter can be estimated regardless of the b value, although is a sensitive method to infer potential thermal pretreatments or changes in the heating rate. It is based on the hypothesis that occupancies of the relevant states remain almost constant for the lowest temperature side of the TL peak and, consequently, this side of the peak will follow an exponential dependence and the applicability of the quasi-equilibrium approximation I_{TL} α exp ($-E_a/kT$), where I_{TL} is the TL intensity, k is the Boltzmann's constant and T is the temperature. Thus, in the Arrhenius plot (ln I_{TL} vs $1/T$), the E_a can be obtained from the slope ($-E_a/k$) (Correcher et al., 2008).

Albite, which is a sodium aluminosilicate ($NaAlSi_3O_8$) that crystalizes with triclinic space group $C\bar{1}$(a = 8.14 Å, b = 13.0 Å, c = 7.19 Å, α = 94.3°, β = 116.5°, ϒ = 87.7°) with developed (110) faces (Li and Knowles, 2013), is usually employed in the field of jewelry, in metallurgical and ceramics industries, as an ornamental stone or gemstone, and more recently, it could be potentially employed as personal dosimeter in case of radiation accident or radiological terrorism where conventional monitoring is not available (Correcher et al., 1999). In this sense, we herein report on the TL properties of an albite from Minas Gerais (Brazil), which has been previously characterized by Raman Spectroscopy and differential thermal analysis (DTA) techniques. The E_a parameter has been calculated from the 10 Gy-induced TL glow curves at each wavelength in the range of 250–500 nm by the IR method.

2. Material and methods

The sample, a natural albite ($NaAlSi_3O_8$) from Minas Gerais (Brazil), was previously studied using X-ray fluorescence (Correcher and Garcia-Guinea, 2013). The characterization has been completed by means of Raman-PL recorded with a Thermo-Fischer DXR Raman-PL Microscope (West Palm Beach, FL 33407, USA) with a point-and-shoot Raman capability of 1 μm spatial resolution. It has been used the 100× objective of the confocal microscope together with a 532 nm laser source delivering 10 mW at 100% laser power mode. The average spectral resolution in the Raman shift ranging from 100 to 5000 cm^{-1} was 4 cm^{-1}, with 900 lines·mm^{-1} grating and 2 μm spot size. The system was operated under OMNIC 1.0 software fitting working conditions such as pinhole aperture of 25 μm, bleaching time 30 s; average of four exposures timed 10 s each. And DTA measurements were carried out using a Model 4851e Mettler Toledo thermal analyzer, using 50 ± 1 mg of each sample and alumina as the reference material that were recorded in a N_2 atmosphere at a heating rate of 10 °C·min^{-1} from room temperature (RT) up to 500 °C. TL measurements were performed on aliquots with 50 μm of diameter and 5.0(1) mg in weight employing an automated Risø TL reader model TL DA-12 provided with an EMI 9635 QA photomultiplier and a $^{90}Sr/^{90}Y$ source with a dose rate of 0.011 Gy s^{-1} calibrated with a ^{137}Cs photon source in a secondary standard laboratory. All TL measurements were analyzed using a linear heating rate of 5 °C·s^{-1} from a RT up to 500 °C in N_2 atmosphere, where the incandescent background was subtracted from TL data. The spectral emission was obtained through a 0.25 mm Ebert monochromator (3 mm slits), where the width of the detection window (λ) is 18 nm at fixed wavelength in the range of 250–500 nm.

3. Results and discussion

3.1. Sample characterization: Raman Spectroscopy and DTA

The characterization of an albite specimen from Minas-Gerais (Brazil) has been carried out by means of Raman spectroscopy and DTA techniques. The Raman spectrum of the sample has been analyzed considering the plot of for end-member feldspars in which three samples of low-T-anorthite- P, low-albite and maximum microcline are outlined (Fig. 1) (Freeman et al., 2008). This model is of interest since allows us to compare different Raman spectra including the five Raman emission peaks groups. The I_a peak position suggests a first-order measurement to distinguish the compositional end members, i.e. 507.6 cm^{-1} in Group I, for the albite sample. Relative intensities of triplet peaks in Group I are an additional criterion to differentiate among feldspar end members. In this vibration type, the displacement of the oxygen atoms of the four-membered ring is seen similar to heart function during the breath, i.e. breathing mode. Oxygen atoms vibrate upright to the T-T line producing differences in the T-O-T angles defining the location of the Group-I Raman peaks. Si-O-Si and Si-O-Al bond angles in albite are classified in three groups clarifying their triplet configuration in the Group-I spectral region. The T-O stretching vibrations of the Group-V from 900 to 1200 cm^{-1} are associated with Si/Al ratios linked to variable amounts of Ca, Na and K in the albite lattice. In accordance with Freeman et al. (2008) and Aliatis et al. (2015), the spectra patterns of albite in Group-IV region are associated with the Al-Si order/disorder of albite lattice exhibiting two sharp peaks circa 760 and 810 cm^{-1} which are probably caused by vibrations of Al-O and Al-O-Si bonds. Groups II and III are less well-explained due to the higher bandwidths. The spectral region of lower wavenumbers, i.e. from 100 to 1100 cm^{-1}, appears as occupied by Raman emission features; on the contrary to the higher wavenumbers (over 1100 cm^{-1}) the sample does not exhibits PL emission.

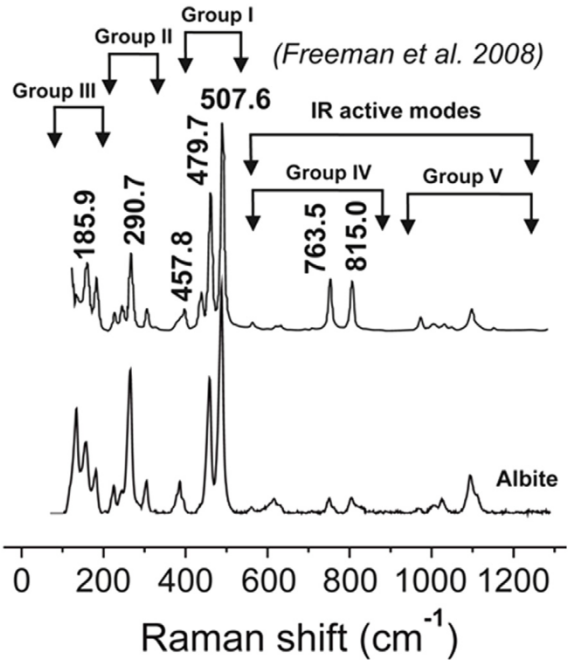

Fig. 1. Raman spectra of an albite from Minas-Gerais (Brazil) and Amelia Court House, Virginia (USA) [26].

Raman spectra collected from in situ heated albite aliquots shows as the most important peaks between 350 and 550 cm^{-1}, at higher temperatures broaden and shift to lower frequencies by 15 to cm^{-1}. Such can be associated with the four-membered tetrahedral ring deformations up to the melting point at 1060 °C (McKeown, 2005). The whole Raman emissions of albite are linked with T-O deformation, compression, breathing, rotation or stretching features; moreover in the main spectral region from 350 to 550 cm^{-1}, sodium atoms are also involved through self-diffusion movements to compensate electric disequilibrium and bonds breakings. In the TL luminescence temperatures range from RT to 500 °C hydroxyl groups also involved in a progressive leaking process from the albite mass.

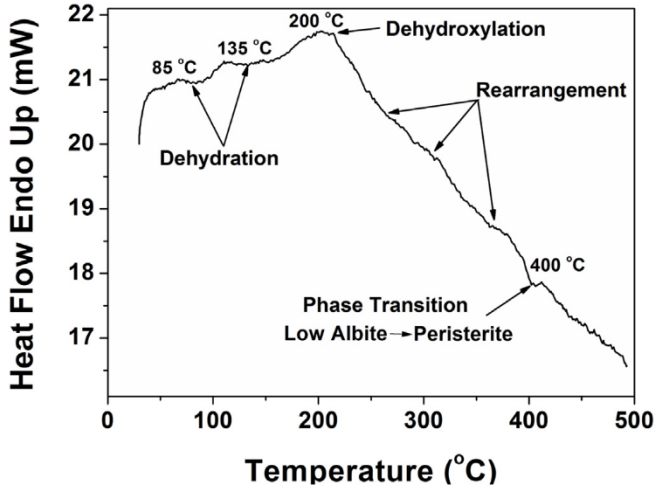

Fig. 2. DTA curve of an albite from Minas-Gerais (Brazil) at a heating rate of 10 °C·min^{-1}.

Additionally, DTA is a sensitive technique to determine endothermic and exothermic processes (i.e. dehydration and dehydroxylation stages, phase transitions and/or redox reactions, among others) (Topaksu et al., 2015). Thus, DTA curve of the natural albite (Fig. 2) exhibits two small endothermic peaks from RT up to 150 °C, centred at 85 and 135 °C, linked to dehydration processes of adsorbed water molecules as appreciated in several silicates (Correcher et al., 2006). At this point, the heat flow increases up to 200 °C in ~5% giving rise an exothermic peak due likely to the presence of Na^+ and oxygen vacancies (O_{2v}*) (Gorobets and Rogojine, 2002) which could react with the environmental water and could form hydroxyl groups that could also be dissociated in OH^- giving rise an exothermic reaction (Greenwood and Earnshaw, 1995; Garcia-Guinea et al., 2017). After the main exothermic reaction, the increase of the temperature induces lattice rearrangement processes in several steps, with a decrease of ~18%, that gives rise to an endothermic effect with a main peak at around 400 °C, which could be due to a phase transition that converts low-albite (in solid solution) into peristerite (Smith, 1970).

3.2. 3D-TL spectral emission

3D-TL plot (Fig. 3) displaying photon intensity (a.u.) against temperature (°C) and wavelength (nm) of the analyzed albite exhibits a

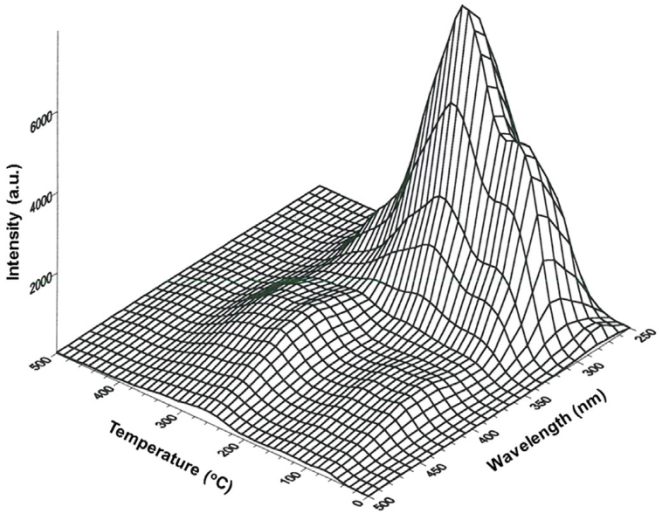

Fig. 3. 3D-TL spectral emission of an albite from Minas-Gerais (Brazil).

complex glow curve where is possible to identify, at least, two wavebands peaked at 290 nm and a broad emission centred at 400 nm that includes four groups of components at 380, 420, 460–500 nm (Correcher et al., 2007b). The higher energy signal (290 nm) is potentially useful in the field of retrospective dosimetry (Correcher et al., 1999) and could be associated with defects-sites due to the recombination process where the diffusion of Na^+ is implicated (Dalal et al., 1988). This behaviour is linked to the thermal effect on the aluminosilicate lattice due to the TL readout that gives rise to alkali self-diffusion through the void channels, redox reactions, consecutive breaking linking of bonds, etc. inducing a continuum in the trap distribution (Correcher et al., 1999). According to Correcher et al. (2007a), the 380 nm waveband is typical of mineral phases containing SiO_4 groups (i.e. silicates and quartz) and could be due to intrinsic defects in the structure, such as, Non-Bridging Oxygen Hole Centers (NBOHCs), $[AlO_4]^o$ centres, alkali planar defects and ionic self-diffusion of alkali atoms and/or Oxygen Defect Centers (ODCs). Otherwise, the broad band peaked at 420 nm, which is common to several feldspars with different chemical compositions and variable Al/Si order, could be associated with the presence of Cu^{2+} next to the hole traps (Dalal et al., 1988) or due to the recombination on a centre formed from a hole-oxygen atom close to two aluminum atoms (Al-O-Al) and Al-O-Si complexes (Speit and Lehmann, 1982). According to Correcher et al. (1999), the lower component in the TL glow curve exhibits a structure associated with a continuous trap distribution, which could be explained as a consequence of a dynamic creation-annihilation of a $[AlO_4/alkali]^+$ and $[AlO_4]^o$ centres due to the ionising radiation effect (10 Gy) that produces a lower yield in the e^--h^+ recombination compared to the 290 nm waveband (intensity ratio of 1:5). On the other hand, the 460–500 nm broad band could be related to the presence of Ti^{4+} (0.74 Å) located in Al^{3+} (0.67 Å) positions where the irradiation scarcely gives rise to a TL signal at 100 °C (Correcher et al., 2007b). The weak green emission at 500 nm would be attributed to the presence of Mn^{2+} (0.81 Å) replacing Na^+ (1.16 Å) and Al^{3+} sites (with coordination number = 6) in the albite crystal lattice (Gaft et al., 2005). Divalent manganese, which is one of the main luminescence activators in feldspars due to the transitions between the different excited states to the corresponding ^6S (A_{1g}) ground state (Tanabe and Sugano, 1954). Thus, considering the Tanabe-Sugano diagram, this emission could be linked to the 3d-3d transitions between the ^4G ($^4T_{2g}$) excited state to the ground state of the Mn^{2+}. The increase of the temperature up to 500 °C induces an emission from 250 to 500 nm at 100 °C directly linked to the ionizing radiation Besides, the 10 Gy-irradiated albite glow curve displays rather broad and complex intensity distributions extending over a significant range of temperatures. Thus, three different spectral regions are apparent and these are tentatively assigned as follows: (i) temperatures values up to 100 °C directly linked to the ionizing radiation; (ii) in the range between 100 °C and 400 °C that could be related to structural defects such as, Na^+ and O_{2v}^* which can react with the environmental water, forming OH^- groups and giving rise to dehydroxylation processes, and to the presence of NBOHCs, ODCs, $[AlO_4]^o$ centres, Al-O-Al and Al-O-Si complexes (characterized by Raman spectroscopy), redox reactions, phase transition (i.e. low albite→peristerite) (detected by DTA) among others; and (iii) there is no signal from 400 °C onwards along the wavelength analyzed due to the background subtraction. Such TL glow curves emission exhibit a very complex structure associated with a continuous trap distribution, which could be explained as a consequence of a dynamic creation-annihilation of a $[AlO_4/alkali]^+$ and $[AlO_4]^o$ centres (Correcher et al., 1999 and 2007b). Furthermore, it is important to mention that the most intense waveband at 290 nm, centred at 180 °C with two maxima peaks at 100 °C and 320 °C and ratio of 1:8:5, appears at temperatures lower than the 400 and 500 nm curves, whose maxima appear close to 260 °C (with ratios of the intensity of 1:4:2 and 1:2:1, respectively). The signal located at 180 °C and 340 nm is more sensitive to the ionizing radiation and could be associated with structural defects, instead of the signal

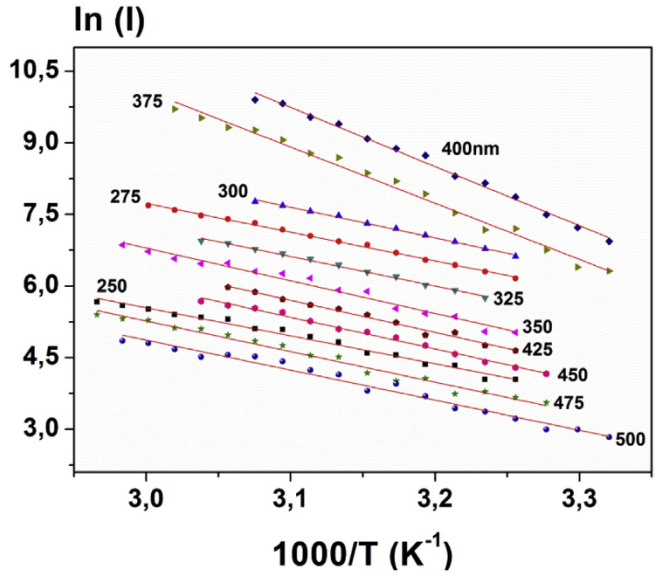

Fig. 4. Arrhenius plot of the 10 Gy irradiated albite from Minas-Gerais (Brazil) in the range of 250–500 nm.

Table 1
Activation energies (E_a in eV) calculated using the IR method performed on 10 Gy-irradiated albite aliquots from 250 to 500 nm; where r is the regression coefficient of linear fitting in the range (in °C) used for the analysis.

Wavelength (nm)	Range (°C)	E_a (eV)	r
250	34–64	0.51 (2)	0.986
275	34–60	0.52 (1)	0.997
300	34–52	0.55 (1)	0.996
325	36–56	0.53 (1)	0.994
350	34–62	0.49 (2)	0.977
375	28–58	0.60 (2)	0.988
400	28–52	0.63 (1)	0.993
425	34–54	0.58 (2)	0.986
450	32–56	0.57 (1)	0.993
475	32–64	0.55 (2)	0.982
500	28–31	0.54 (2)	0.978

which appears at higher temperatures (260 °C) at 400 nm, which is more sensitive to the point defects in the albite lattice structure.

3.3. Initial rise method

Based on the 10 Gy-induced TL spectral emission of the analyzed plagioclase, one can estimate the Arrhenius plot of the low-T side (ln I vs 1000/T) at each wavelength (from 250 to 500 nm) (Fig. 4), where the E_a parameter can be determined from the slope (E_a/k) by means of the IR method (Chen and McKeever, 1997). Table 1 allows us to distinguish, at least, three groups of components taking into account the E_a values namely: (i) in the range of 250–350 nm where the evolution of the E_a remains constant (~0.5 eV) due to the presence of the Na^+ in the lattice; (ii) a second group in the range of 375–400 nm where E_a values are close to ~ 0.6 eV. Such increase would indicate that the luminescence emission is linked to structural defects, as abovementioned that dominates over the rest of the processes. And, (iii) a third group in the range of 425–500 nm, where the E_a value are close to ~ 0.56 eV, that could be linked to redox reactions of Cu (6 ppm), Ti (0.09%) and Mn (0.02%) ions (Correcher et al., 2007b) and/or the presence of Al-O-Al and Al-O-Si complexes. All of the IR analyses follow a simple linear regression that fits linearly with acceptable r coefficients ($r > 0.977$), where the assessment of the E_a for each TL waveband reveals the presence of traps with similar depth for the first (250–350 nm) and third (425–500 nm) group of components (mainly linked to point defects), that does not appears for the second (375–400 nm) group of components which can be mostly related to structural defects.

4. Conclusions

The natural Na-rich aluminosilicate here studied displays a complex UV-green 3D-TL spectrum of, at least, five wavebands peaked at 290, 380, 420, 460 and 500 nm. They could be linked mainly to structural and occasionally point defects, namely: (i) a large flat emission of multi-order kinetics at 290 nm associated with defects-sites due to the presence of the Na ions in the lattice; (ii) the UV-blue emission band at 380 nm, characteristic of mineral phases with SiO_4 groups, linked to intrinsic defects in the structure (i.e. NBOHCs, ODCs, $[AlO_4]^o$ centres, alkali planar defects, among others); (iii) the 420 nm band could be due to the recombination on a centre formed from the Al-O-Al and Al-O-Si complexes; (iv) the 460 nm broad waveband is associated with the presence of Ti^{4+} in the sample; and (v) the 500 nm band could be linked to Mn^{2+} point defects in the albite crystal lattice. The estimation of E_a values for the 10 Gy-induced TL glow curves analyzed by means of IR method reveal three groups of components (shallower traps) at different depth in the range of 0.49(2)-0.63(1) eV.

Acknowledgments

Cecilia Boronat thanks to “Consejería de Educación, Juventud y Deporte de la Comunidad de Madrid, Spain” and “Fondo Social Europeo, Belgium” (PEJ15/BIO/AI-0418) for the support provided under the “Operativo de Empleo Juvenil y la Iniciativa de Empleo Juvenil (YEI)” program (B.O.C.M. Núm.152. Orden 1880/2015, de 16 de junio del 2015).

References

Aitken, M.J., 1985. Thermoluminescence Dating. Academic Press, Orlando, Florida (USA).

Aliatis, I., Lambruschi, E., Mantovani, L., Bersani, D., Ando, S., Diego Gatta, G., Gentile, P., Salvioli-Mariani, E., Prencipe, M., Tribaudino, M., Lottici, P.P., 2015. A comparison between ab initio calculated and measured Raman spectrum of triclinic albite (NaAlSi3O8). J. Raman Spectrosc. 46, 501–508. https://doi.org/10.1002/jrs.4670.

Almeida, S.B., Villani, D., Sakuraba, R.K., Rezende, A.C.P., Campos, L.L., 2018. TL and OSL dosimetric characterization of different luminescent materials for clinical electron beams application in TSEB treatments. J. Lumin. 198, 497–501. https://doi.org/10.1016/j.jlumin.2018.02.065.

Aslar, E., Sahiner, E., Polymeris, G.S., Meric, N., 2017. Determination of trapping parameters in BeO ceramics in both quenched as well as reconstructed thermoluminescence glow curves using various analysis methods. Appl. Radiat. Isot. 129, 142–151. https://doi.org/10.1016/j.apradiso.2017.08.0268.

Bailiff, I.K., Stepanenko, V.F., Goksu, H.Y., Botter-Jensen, L., Brodski, L., Chumak, V., Correcher, V., Delgado, A., Golikov, V., Jungner, H., Khamidova, L.G., Kolizshenkov, T.V., Likhtarev, I., Meckbach, R., Petrov, S.A., Sholom, S., 2004. Comparison of retrospective luminescence dosimetry with computational modeling in two highly contaminated settlements downwind of the chernobyl NPP. Health Phys. 86, 25–41. https://doi.org/10.1097/00004032-200401000-00006.

Bailiff, I.K., Stepanenko, V.F., Goksu, H.Y., Botter-Jensen, L., Correcher, V., Delgado, A., Golikov, V., Jungner, H., Khamidova, L.G., Kolizshenkov, T.V., Meckbach, R., Petin, D.V., Orlov, M.Y., Petrov, S.A., 2005. Retrospective luminescence dosimetry: development of approaches to application in populated areas downwind of the Chernobyl NPP Health. Phys 89, 233–246. https://doi.org/10.1097/01.HP.0000164654.66585.20.

Chen, R., McKeever, S.W.S., 1997. Theory of Thermoluminescence and Related Phenomena. World Scientific, Singapore. https://doi.org/10.1142/2781.

Correcher, V., Garcia-Guinea, J., 2013. UV-induced blue thermoluminescence of annealed Na-rich aluminosilicates. Radiat. Meas. 56, 244–247. https://doi.org/10.1016/j.radmeas.2013.03.008.

Correcher, V., Garcia-Guinea, J., Castillejo, M., Oujja, M., Rebollar, E., Lopez-Arce, P., 2006. Laser-induced fluorescence and thermoluminescence response of a Na-Ca rich silicate. Radiat. Meas. 41, 971–975. https://doi.org/10.1016/j.radmeas.2006.05.004.

Correcher, V., Garcia-Guinea, J., Martin-Fernandez, C., Can, N., 2011. Thermal effect on the cathodo- and thermoluminescence emission of natural topaz ($Al_2SiO_4(F,OH)_2$). Spectrosc. Lett. 44, 486–489. https://doi.org/10.1080/00387010.2011.610405.

Correcher, V., Garcia-Guinea, J., Sanchez-Munoz, L., Rivera, T., 2007b. Luminescence characterization of a sodium-rich feldspar. Radiat. Eff. Defect Solid 162, 709–714. https://doi.org/10.1080/10420150701482063.

Correcher, V., Gomez-Ros, J.M., Delgado, A., 1999. Use of albite as a dosemeter in

accident dose reconstruction. Radiat. Protect. Dosim. 84, 547–549. https://doi.org/10.1093/oxfordjournals.rpd.a032795.
Correcher, V., Gomez-Ros, J.M., Garcia-Guinea, J., 2004. Radiation effect on the 400-nm-thermoluminescence emission of a potassium-rich feldspar. Radiat. Meas. 38, 689–693. https://doi.org/10.1016/j.radmeas.2003.12.006.
Correcher, V., Gomez-Ros, J.M., Garcia-Guinea, J., Lis, M., Sanchez-Munoz, L., 2008. Calculation of the activation energy in a continuous trap distribution system of a charoite silicate using initial rise and TL glow curve fitting methods. Radiat. Meas. 43, 269–272. https://doi.org/10.1016/j.radmeas.2007.10.032.
Correcher, V., Sanchez-Munoz, L., Garcia-Guinea, J., Benavente, D., Delgado, A., 2007a. Comparison of UV-IR radioluminescence and cathodoluminescence spectra of a potassium feldspar. Radiat. Meas. 42, 780–783. https://doi.org/10.1016/j.radmeas.2007.02.013.
Cruz-Zaragoza, E., Roman-Lopez, J., Cordoba, D.R., Furetta, C., Santiago, M., Marcazzo, J., 2015. Luminescence detection and dose assessment of irradiated Yerba Mate (Ilex paraguariensis) tea leaves. Appl. Radiat. Isot. 100, 75–78. https://doi.org/10.1016/j.apradiso.2014.11.022.
Dalal, M.L., Kirsh, Y., Rendell, H.M., Townsend, P.D., 1988. TL emission-spectra of natural feldspar. Nucl. Tracks Radiat. Meas. 14, 57–62.
Freeman, J.J., Wang, A., Kuebler, K.E., Jolliff, B.L., Haskin, L.A., 2008. Characterization of natural feldspars by Raman spectroscopy for future planetary exploration. Can. Mineral. 46, 1477–1500. https://doi.org/10.3749/canmin.46.6.1477.
Gaft, G., Reisfeld, R., Panczer, G., 2005. Modern Luminescence Spectroscopy of Minerals and Materials. Springer-Verlag Berlin Heidelberg. https://doi.org/10.1007/b137490.
Garcia-Guinea, J., Garrido, F., Lopez-Arce, P., Correcher, V., de la Figuera, J., 2017. Spectral green cathodoluminescence emission from surfaces of insulators with metal-hydroxyl bonds. J. Lumin. 190, 128–135. https://doi.org/10.1016/j.jlumin.2017.05.039.
Gomez-Ros, J.M., Correcher, V., Garcia-Guinea, J., Delgado, A., 2002. Kinetic parameters of lithium and aluminium doped quartz from thermoluminescence glow curves. Radiat. Protect. Dosim. 100, 399–402.
Gonzalez, M., Correcher, V., 2014. On the cathodoluminescence and thermoluminescence emission of lithium titanate ceramics. J. Nucl. Mater. 445, 149–153. https://doi.org/10.1016/j.jnucmat.2013.10.062.
Gorobets, B.S., Rogojine, A.A., 2002. Luminescent Spectra of Minerals. RPC VIMS, Moscow, Russia.
Greenwood, N.N., Earnshaw, A., 1995. Chemistry of the Elements. https://doi.org/10.1016/S0277-5387(00)84180-7.
Jeong, H., Park, M., Jeong, H., Hwang, W., Kim, E., Han, M., 2013. Radiological risk assessment caused by RDD terrorism in an urban area. Appl. Radiat. Isot. 79, 1–4. https://doi.org/10.1016/j.apradiso.2013.04.018.
Kalita, J.M., Chithambo, M.L., 2017. Thermoluminescence of alpha-Al2O3:C,Mg: kinetic analysis of the main glow peak. J. Lumin. 182, 177–182. https://doi.org/10.1016/j.jlumin.2016.10.031.
Keskin, I.C., Kati, M.I., Turemis, M., Cetin, A., Arslanlar, Y.T., Kibar, R., 2018. Determination of thermoluminescence kinetic parameters of white and blue chalcedony exposed to X-ray irradiation. Radiat. Phys. Chem. 151, 114–119. https://doi.org/10.1016/j.radphyschem.2018.05.031.
Krbetschek, M.R.R., Götze, J., Dietrich, A., Trautmann, T., 1997. Spectral information from minerals relevant for luminescence dating. Radiat. Meas. 27, 695–748. https://doi.org/10.1016/S1350-4487(97)00223-0.
Li, B., Knowles, K.M., 2013. Molecular dynamics simulation of albite twinning and pericline twinning in low albite. Model. Simul. Mater. Sci. Eng. 21 (5), 055012 Art. https://doi.org/10.1088/0965-0393/21/5/055012.
McKeever, S.W.S., 1986. Mechanisms of thermoluminescence production in materials for radiation dosimetry. Radiat. Protect. Dosim. 17, 431–435. https://doi.org/10.1093/oxfordjournals.rpd.a032865.
McKeown, D.A., 2005. Raman spectroscopy and vibrational analyses of albite: from 25 °C through the melting temperature. Am. Mineral. 90, 1506–1517. https://doi.org/10.2138/am.2005.1726.
Muñiz, J.L., Delgado, A., Gomez-Ros, J.M., Brosed, A., 1995. Application of glow curve analysis methods to radiotherapy mailed dosimetry with LiF TLD-100. Phys. Med. Biol. 40 253-26. https://doi.org/10.1088/0031-9155/40/2/004.
Rodriguez-Lazcano, Y., Correcher, V., Garcia-Guinea, J., Cruz-Zaragoza, E., 2013. Gamma radiation-induced thermoluminescence emission of minerals adhered to Mexican sesame seeds. Radiat. Phys. Chem. 83, 15–18. https://doi.org/10.1016/j.radphyschem.2012.09.017.
Smith, J.V., 1970. Physical properties of order-disorder structures with especial reference to feldspar minerals. Lithos 3, 145–160. https://doi.org/10.1016/0024-4937(70)90070-8.
Speit, B., Lehmann, G., 1982. A comparative study of thermoluminescence and isothermal destruction of radiation defects in feldspars. J. Lumin. 27, 127–136. https://doi.org/10.1016/0022-2313(82)90014-X.
Tanabe, Y., Sugano, S., 1954. On the absorption spectra of complex ions .1. J. Phys. Soc. Jap. 9, 753–766. https://doi.org/10.1143/JPSJ.9.753.
Topaksu, M., Correcher, V., Garcia-Guinea, J., Yuksel, M., 2015. Effect of heating rate on the thermoluminescence and thermal properties of natural ulexite. Appl. Radiat. Isot. 95, 222–225. https://doi.org/10.1016/j.apradiso.2014.10.020.